High-Energy X-Ray Microscopy at the National Ignition Facility

J. A. Koch *C. Brown** *S. G. Glendinning* *D. H. Kalantar*

T. W. Barbee, Jr. *P. Celliers* *B. A. Hammel* *O. L. Landen*

G. R. Bennett† *L. B. Da Silva* *W. Hsing*† *J. Seely**

Introduction

X-ray microscopy has made numerous critical contributions to the current state of knowledge in inertial confinement fusion (ICF) research[1] and in other areas of laser-produced plasma research, and we expect it to continue to be vital for experiments at the National Ignition Facility (NIF). Examples of experiments relying on high-energy, high-resolution microscopy include backlit shock radiography for diagnosis of time-dependent radiation symmetry in hohlraums,[2] emission imaging of doped ICF capsules for diagnosis of temperature and density uniformity in the compressed core,[3] and shock trajectory measurements for equation-of-state studies.[4,5]

Detector-mounted pinholes and slits are typically used in experiments at Nova and at other facilities. However, the extreme environment at NIF implies that there will be an exclusion zone with a radius of ~200 mm, inside of which pinholes and associated shielding mounted to the detector may not survive high-energy experiments. This distance is farther than desired for pinhole imaging due to diffractive degradation of spatial resolution and to decreased collection solid angles for a fixed magnification.

In anticipation of experiments at NIF, we have begun a systematic investigation of various options for x-ray imaging at energies of ~4–13 keV. X-ray sources in this spectral region are generally line emitters, and this implies that high efficiency is needed only over a relatively narrow spectral region containing the emission line of interest. However, various emission lines at different energies are of interest, and this implies that quasi-monochromatic x-ray imaging instruments should have flexibility in operating energy. In addition, minimization of neutron and high-energy x-ray backgrounds implies that the x-ray detector should ideally be shielded from a direct line of sight to the target, and also implies that at least a moderate spectral selectivity is desirable. The experiments envisaged here have different requirements, but typically include 0.5- to 2-mm fields of view in one or two dimensions, suitability for multiple-frame imaging onto a gated camera for 2D applications, 2- to 10-μm spatial resolution at the source, magnifications of 4–40×, and high efficiency for both emission and absorption geometries.

The options being considered fall into two categories. The first category is short-working-distance, expendable imaging elements, and includes primarily pinholes and their 1D analog, slits. Pinholes have proven to be versatile and simple to use; however, to operate at NIF with useful collection angle and spatial resolution, the pinhole must be mounted well within the exclusion zone, with the result that the pinhole and associated support structure will likely be destroyed during the experiment. One solution is to mount the pinhole on the target rather than on the detector; however, this will add an extra source of exploding debris to the target that could also damage detectors and could damage laser optics. In addition, premature pinhole closure during the experiment is a concern.[6] Possible options include tamping the pinhole with plastic to mitigate closure during the experiment, and placing a plastic wedge on the target side of the pinhole in order to control its trajectory. Reduced image contrast due to a high-energy x-ray background transmitted through the substrate may also be an issue for some experiments.

The second category is long-working-distance, reusable diagnostics that are designed to survive high-energy experiments, and this category includes primarily reflective-optic imaging systems. Types of imaging systems being considered include metal–mirror Kirkpatrick–Baez (KB) microscopes,[7] multilayer mirror

*Naval Research Laboratory, Washington, DC
†Los Alamos National Laboratory, Los Alamos, NM

KB microscopes,[8] bent-crystal KB microscopes, single spherical[9] or toroidal[10] crystal microscopes, and dual spherical-crystal microscopes.[11] More complex compound grazing-incidence systems could also be considered, such as Wölter's and similar variations,[12,13] but in any case versatility, simplicity of alignment, and cost are vital practical considerations.

Our current strategy is to investigate short-working-distance, target-mounted pinholes in Nova experiments while simultaneously investigating reflective optic imaging systems for long-term implementation at NIF. The variety of design options is large, and we begin by systematically investigating the advantages and disadvantages of the simplest reflective optic systems and comparing them to pinholes and slits. We note that the image exposure (e.g., in W/cm^2) obtained on a detector by an imaging system can be written generally as $(\Omega\eta/M_vM_h)I_0$, where I_0 is the spectrally integrated source brightness (e.g., in W/cm^2*Sr), M_v and M_h are the vertical and horizontal magnifications, Ω is the collection solid angle, and η is the collection efficiency including any losses due to reflectivity or bandwidth limitations. The scaled image brightness $\Omega\eta/M_vM_h$ (units of Sr), achievable while meeting a specified requirement for source spatial resolution over a given field of view (FOV), therefore serves as a figure of merit with which to weigh the various options.

Calculations and Results

In a detailed separate paper,[14] we have investigated the achievable image brightness for several options in various configurations using analytical derivations backed by numerical ray tracing. There, we used a geometrical optics analysis to estimate Ω and η for 1D and 2D imaging near 6 keV with the Mn K-α (E = 5.9 keV, $\lambda/\Delta\lambda \approx 200$) and the Mn He-$\alpha$ (E = 6.15 keV, $\lambda/\Delta\lambda \approx 2000$), comparing the achievable image brightness for an Ir mirror KB; a multilayer mirror KB;[15] a depth-graded multilayer mirror KB;[15] a bent-crystal KB using mica in 3rd order,[16] Si (220) [Ref. 17], LiF (220) [Ref. 17], and Si (422) [Ref. 17]; and a spherical crystal using Si (422) [Ref. 17], CaF_2 (111) in 3rd order[16] and quartz 22$\underline{4}$3.[18] In this paper we present only the results, and refer the interested reader to Ref. 14 for further details.

In Figures 1 and 2 we plot the estimated image brightness for 2D imagers using the Mn K-α source and the Mn He-α source, respectively, assuming a 200-mm source/optic distance and a magnification M = 4, while maintaining a spatial resolution better than 10 μm throughout a 2-mm FOV. For comparison, we also plot the estimated image brightness for an 8-μm-diam pinhole operating at M = 4 with a *detector* distance of 200 mm. In Figures 3 and 4 we plot the estimated image brightness for 1D imagers using the Mn K-α source and the Mn He-α source, respectively, assuming a 200-mm source/optic distance and a magnification M = 40 in the spatially resolved dimension, while maintaining a spatial resolution better than 3 μm throughout a 0.3-mm FOV and integrating over a 0.3-mm region in the nonimaged dimension of the target. For comparison, we also plot the estimated image brightness for a 2.8-μm-wide slit operating at M = 30 with a *detector* distance of 200 mm. Those instruments that are not capable of achieving the required FOVs due to reflector or source bandwidth limits (discussed later) are shown as open circles or triangles in all cases.

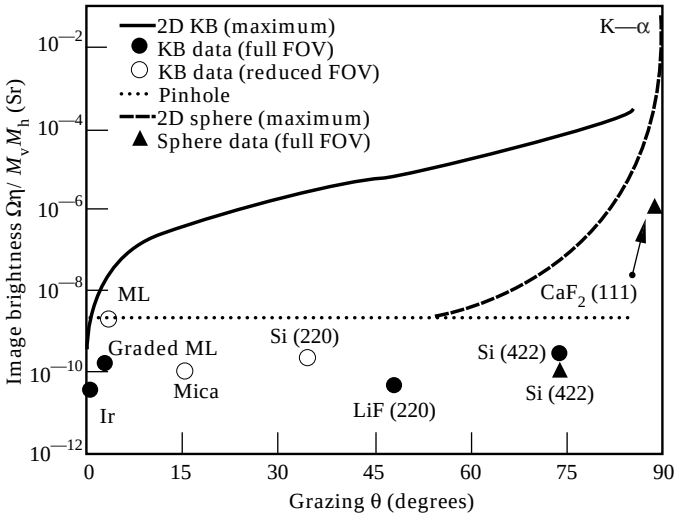

FIGURE 1. Estimated image brightness for several choices of 2D imaging microscope configurations and mirror materials assuming the Mn K-α line is used for imaging. (08-00-0598-1166pb01)

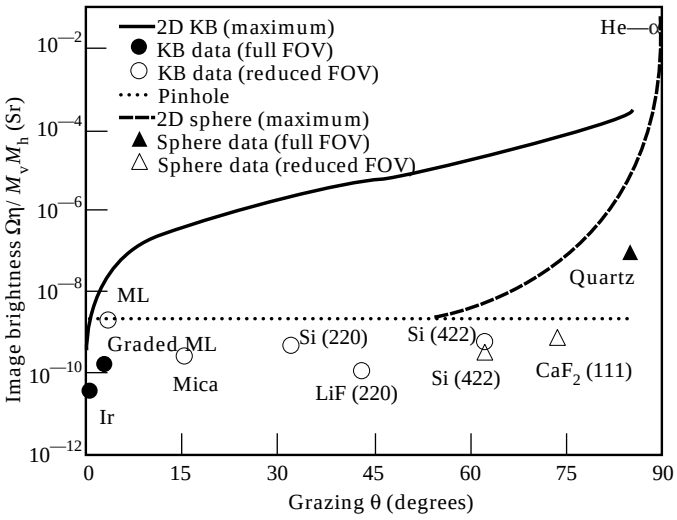

FIGURE 2. Estimated image brightness for several choices of 2D imaging microscope configurations and mirror materials assuming the Mn He-α line is used for imaging. (08-00-0598-1167pb01)

We first discuss the results for 2D microscopes. As Figures 1 and 2 show, metal–mirror KB systems generally provide low image brightness compared with other designs for the parameters considered, primarily due to severe obliquity that necessitates small solid angles in order to maintain the desired resolution over the FOV. In addition, surface roughness becomes an increasing problem for higher photon energies, and this can degrade resolution by producing diffuse scattering.

For the parameters considered, a KB using conventional multilayer mirrors is more efficient than one using depth-graded multilayer mirrors. This is because the bandpass of the conventional multilayer mirror is sufficient to avoid chromatic vignetting of the collection angle, caused by the variation in the angle of incidence θ across the mirror surface, while providing a peak reflectivity that is a factor of ~4 higher than the depth-graded mirror. We note that in the bent-crystal KB systems, the integrated reflectivity of each crystal considered is small compared with that of a multilayer mirror, and the increased geometrical solid angles achievable at larger θ are more than offset by decreased efficiency, resulting in low image brightness for all bent-crystal KBs investigated.

It is clear in principle from Figures 1 and 2 that for the 2D imaging cases we consider here, spherical crystals operating within ~5–10° of normal incidence meet the specified requirements for source resolution over a specified FOV while providing the highest efficiency of any system considered. This is because the geometrical optics-limited collection angle is relatively large near normal incidence, because chromatic vignetting of the collection angle is less important near normal incidence since θ varies less across the aperture, and because there is only one reduction in image brightness for crystal efficiency. Indeed, we note that a two-crystal KB using Si 422 mirrors yields an image brightness only slightly higher than that obtained with a single Si 422 spherical crystal, despite the fact that the angle of incidence is far from normal (~65–70 degrees) and that the geometrical aberration-limited collection angle of the KB is much greater than that of the spherical mirror. Compared with multiple-crystal compound systems,[11] the use of toroidal crystals may generally be a more efficient means of increasing image brightness for off-normal angles of incidence by minimizing astigmatism and allowing larger apertures to be used.

While the collection solid angle of a pinhole is small, it has an efficiency of unity, and, for the parameters considered, the near-normal-incidence spherical crystals are the only systems that yield an image brightness larger than that obtainable with the chosen short-working-distance pinhole. Pinholes have compensating disadvantages, however, including possible closure during the experiment,[6] increased parallax across multiple-frame images, and high-energy x-ray transmission through the substrate. The last problem could be alleviated by the use of flat multilayer mirrors to reflect the image onto the detector, potentially eliminating a direct line of sight from the detector to the target.[19]

Many of the above comments also apply to the 1D imaging results of Figures 3 and 4. The image brightness of all bent-crystal KB systems are relatively low compared with the other systems considered, and are generally even lower than the Ir-mirror KB. However, in the 1D imaging case, the conventional multilayer KB yields an image brightness higher than any spherical

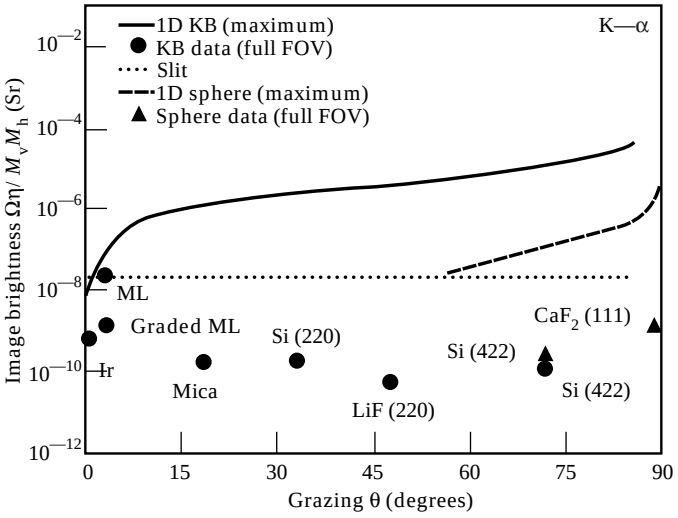

FIGURE 3. Estimated image brightness for several choices of 1D imaging microscope configurations and mirror materials assuming the Mn K-α line is used for imaging. (08-00-0598-1168pb01)

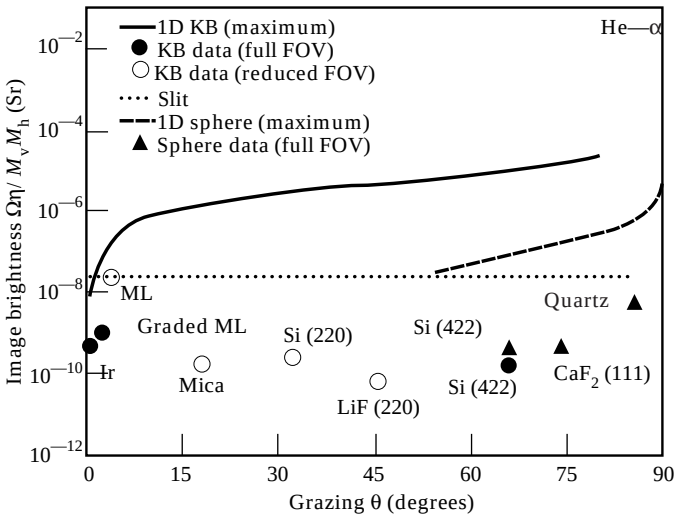

FIGURE 4. Estimated image brightness for several choices of 1D imaging microscope configurations and mirror materials assuming the Mn He-α line is used for imaging. (08-00-0598-1169pb01)

crystal considered, by a factor >10. Much of this increase is due to the fact that the horizontal KB mirror is configured in this system to operate at $M = 1$, while the spherical crystal must operate with $M = 40$ in both dimensions. In addition, the choice of $M = 1$ eliminates chromatic vignetting of the collection angle in the horizontal dimension because the angles of incidence for all rays from an on-axis source point are equal, thus allowing the full (large) horizontal aperture to be used. We note that a toroidal bent crystal is unlikely to yield a significant increase in image brightness for 1D imaging because high resolution is required in one dimension only. However, the spherical crystal retains the significant practical advantage of simplicity, and the reduction in image brightness is likely to be tolerable in many cases provided the spherical crystal can actually meet the 3-μm source resolution requirement.

The chosen short-working-distance slit in Figures 3 and 4 yields an image brightness equal to or larger than that attainable with any reflective-optic imaging system considered. However, the compensating disadvantages of the pinhole also apply to the slit, and are in fact more significant here because the working distance is very short and the required slit width is very small. Slit closure problems could be minimized by moving the slit and detector farther from the target, at the cost of reduced image brightness and more significant diffraction limitations.

Discussion and Conclusions

It appears that spherical or toroidal crystals may be the most promising general options for high-energy x-ray microscopy applications at NIF. These optics can provide high throughput for 2D applications and can also provide good throughput for 1D applications, provided the operating wavelength matches a useful emission line and provided the bent crystal quality is high. Their simplicity is also attractive, particularly for 2D applications requiring multiple images onto gated microchannel-plate strips. Due to the low integrated reflectivity of most useful high-resolution imaging crystals, toroidal crystals are apparently a more efficient means of increasing collection angles for off-normal angles of incidence than compound-crystal systems.

Multilayer KB systems using spherical mirrors appear to be good options for 1D applications requiring high spatial resolution over narrow FOVs, and are most efficient when mirror bandwidths are just large enough to avoid chromatic vignetting of the collection angle while maintaining the highest possible peak reflectivity. These systems are also good secondary options for 2D applications. More complex multiple-optic compound systems might allow larger collection angles to be used provided the mirror bandwidths are sufficiently large, but their net advantages would have to be weighed against their significant added complexity and cost, particularly for 2D imaging applications.

It is clear from Figures 1 through 4 that in many cases, the specified FOV cannot be achieved with bent-crystal KB systems or conventional multilayer-coated mirrors, and in some cases cannot be achieved even with near-normal-incidence crystals. This is due to chromatic vignetting of the FOV, caused by finite source linewidths and mirror bandwidths, and is particularly significant with the narrowband He-α source in Figures 2 and 4. For example, the maximum FOV of the multilayer mirror KB is ≈0.3 mm in all cases; mica, Si (220), LiF (220), and Si (422) bent-crystal KBs in Figures 2 and 4 have maximum FOVs of 0.06, 0.12, 0.2, and 0.4 mm respectively; and the CaF_2 (111) spherical crystal in Figures 2 and 4 has a maximum FOV of 0.7 mm. This obstacle to further Bragg reflector microscope development could be avoided by introducing apertures on the detector side of the mirrors, as illustrated in Figure 5. Here, the aperture is placed along the chief on-axis reflected ray at a distance $x = 2f$ from the mirror, where $f = Mp/(M + 1)$. The aperture width is chosen to limit the collection solid angle, while the mirror dimension limits the FOV. This geometry is similar to that used in a high-resolution metal–mirror KB microscope at Lawrence Livermore National Laboratory,[5] where the backlight source was placed on the Rowland circle and the backlight diameter limited the collection solid angle and therefore determined the spatial resolution. However, as noted above, backlit imaging with the source on the Rowland circle will generally be impossible at NIF due to limited flexibility in laser beam pointing. The aperture technique described here does not require a backlight source on the Rowland circle, does not place any limitations on backlight dimensions, and can

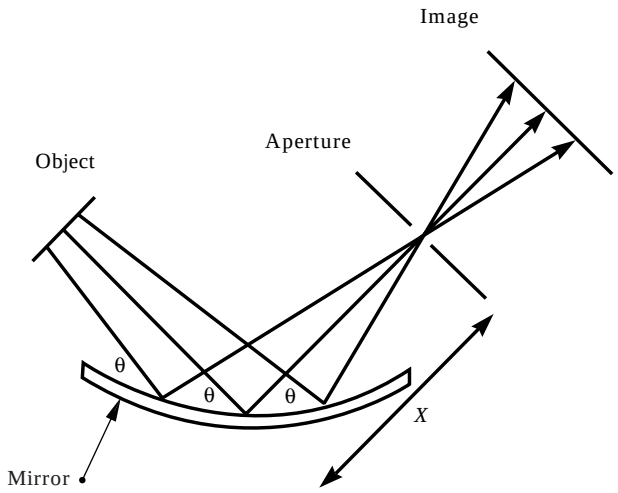

FIGURE 5. Sketch showing how an aperture, placed behind a mirror on the Rowland circle, can be used to minimize chromatic vignetting of the FOV with Bragg reflector mirrors. (08-00-0598-1170pb01)

be used for emission imaging. Further research is required in order to determine the geometrical limitations to the aperture width and thus the collection angle for this geometry.

The general utility of near-normal-incidence spherical or toroidal crystals for high-energy x-ray imaging at NIF and similar future facilities will depend on two main factors. The first is the limited choice of operating wavelengths, dictated by the requirement that θ be near 90° and by the limited number of useful crystal planes. We have begun a systematic search for matches between desirable source emission lines and crystal planes; however, further research will be required in order to determine the actual 2d spacings and integrated reflectivities for these crystals while bent to spherical or toroidal shapes. The second limiting factor for spherical crystal imaging is crystal quality. For high-resolution imaging applications, crystal perfection must be high, because mosaic structure will result in degraded spatial resolution; only highly perfect crystals can be used, and this factor will further limit the choices of operating wavelengths for spherical or toroidal crystals. Additionally, the mechanical properties of bent crystals are also important, as the crystals must retain high perfection while bent to spherical or toroidal shapes. Further research is required in order to assess these issues for specific crystal choices.

Acknowledgment

We gratefully acknowledge the contributions and support of M. Cable, R. Cauble, G. Collins, U. Feldman, J. Kilkenny, B. Remington, and J. Trebes.

References

1. J. Lindl, *Phys. Plasmas* **2**, 3933–4024 (1995).
2. P. Amendt et al., *Rev. Sci. Instrum*. **66**, 785–787 (1995).
3. I. Uschman et al., *Rev. Sci. Instrum*. **66**, 734–736 (1995).
4. B. A. Hammel et al., *Phys. Fluids B* **5**, 2259–2264 (1993).
5. L. B. Da Silva et al., *Phys. Rev. Lett*. **78**, 483–486 (1997).
6. B. A. Remington et al., *Rev. Sci. Instrum*. **63**, 5080–5082 (1992).
7. F. J. Marshall and Q. Su, *Rev. Sci. Instrum*. **66**, 725–727 (1995).
8. J. H. Underwood et al., *Rev. Sci. Instrum*. **67**, 1–6 (1996).
9. C. Brown et al., *Rev. Sci. Instrum*. **68**, 1099–1102 (1997).
10. M. Dirksmöller et al., *Opt. Comm*. **118**, 379–387 (1995).
11. E. Förster et al., *Exp. Tech. Physics* **42**, 19–24 (1996).
12. H. Wölter, *Ann. Physik* **10**, 94–114 (1952).
13. R. Kodama et al., *Opt. Lett*. **21**, 1321–1323 (1996).
14. J. A. Koch et al., *Appl. Opt*. (in press).
15. J. F. Seely et al., *Appl. Opt*. **35**, 4408–4412 (1996).
16. H. T. Yamada et al., Lawrence Berkeley National Laboratory, Berkeley, CA, Report No. LBL-22800 (1986).
17. B. L. Henke, E. M. Gullikson, and J. C. Davis, *Atomic Data and Nuc. Tables* **54** (2) (1993).
18. N. G. Alexandropolous and G. C. Cohen, *Appl. Spectrosc*. **28**, 155–164 (1974).
19. J. L. Bourgade et al., *Plasma Phys. Rep*. **20**, 107–112 (1994).